Lunar magnetic field evidence for Imbrian-aged dike emplacement in the South Pole-Aitken basin: Interpretation of new maps of the internal and external fields

Michael E. Purucker

Raytheon at Planetary Geodynamics Laboratory, NASA/GSFC, Greenbelt, Maryland, USA

Terence J. Sabaka

Raytheon at Planetary Geodynamics Laboratory, NASA/GSFC, Greenbelt, Maryland, USA

James W. Head III

Brown University, Providence, Rhode Island, USA

Nikolai A Tsyganenko

USRA at Goddard Space Flight Center, NASA, Greenbelt, Maryland, USA

Nils Olsen

Danish National Space Center, Copenhagen, Denmark

Jasper S. Halekas

Space Sciences Laboratory, University of California-Berkeley,Berkeley, California, USA

Mario H. Acuña

[14] Goddard Space Flight Center, NASA, Greenbelt, Maryland, USA

Lionel Wilson

[15] Lancaster University, Lancaster, UK

Abstract. A new lunar magnetic field parameterization, which allows solution for both external and internal fields in the near-lunar magnetic field environment, has revealed cross-cutting field structures from Lunar Prospector observations over the South Pole-Aitken basin. These linear features are, in part, co-located with a farside occurrence of mare ponds that represent a series of eruptions of mantle-derived basaltic magma onto the surface, and lava flooding and solidification in low regions. The linear magnetic anomalies are interpreted to be magnetized dike systems intruded into the crust that fed the surface eruptions producing the mare basalt ponds. Such an origin would require that there be a magnetic field present for part of the period spanning the dikes/mare ponds emplacement. Estimates of the age of the mare ponds (Late Imbrian) are consistent with the period in lunar history during which a magnetic field of peak strength is thought to have been present.

1. Introduction

The mapping of magnetic fields has proven to be a useful tool for providing a 3rd dimension to surface observations of the earth's composition and geologic structure. A suite of mathematical techniques has been developed [*Blakely*, 1995] to facilitate the interpretation of these fields. Application of these techniques to the moon may permit new insights into the geologic processes acting there.

The magnetic anomalies of the South Pole-Aitken (SPA) basin region have previously been interpreted to be of impact origin by virtue of their locations approximately antipodal to the Imbrium, Serenitatis, and Crisium basins [*Hood et al.*, 2001]. Our new analysis reveals the presence of linear crustal magnetic anomalies co-located in part with abundant lunar mare ponds and is consistent with the anomalies representing magnetized linear dikes that fed these eruptions.

2. Data

Lunar Prospector vector fluxgate magnetometer data from December of 1998 through July of 1999 were utilized here. The selenographic data were first converted to a local spherical coordinate system with the usual definition of B_r positive outward, B_θ positive southward, and B_ϕ positive eastward. Observations were collected at a range of altitudes between 18 and 46 km. The electron reflectometer data [*Halekas et al.*, 2001], which also contain information on the Lunar crustal field, were not utilized in the present study, but we discuss our interpretations in light of these data.

3. Model

3.1. External Magnetic Field

Prior to the analysis of the internal magnetic field, we developed a simple model of the external magnetic field and removed it from the Lunar Prospector observations. After separating the data into half-orbits, extending from north to south pole, a uniform external field was determined using all three components of the vector data, from the part of the orbits when Lunar Prospector was in the Earth's magnetotail. This approach, widely used in the construction of maps of the Earth's magnetic field [*Maus et al.*, 2006], differs from the component by component, quadratic detrending approach of *Hood et al.* [2001] in treating the external field as a potential field. The external field directions and intensities deduced using this approach were compared with the standard T96 model of the Earth's magnetosphere [*Tsyganenko*, 1996]. Shown in Figure 1 are the magnetic field vectors predicted from Lunar Prospector data in red and the geodipole plus T96 model in blue for tail encounters in 1999 when the subsatellite track of Lunar Prospector took it over the SPA region. Both northern, and southern magnetotail lobes are represented, as is the plasma sheet. The T96 model vectors in Figure 1 were calculated using concurrent observations of the interplanetary medium by the ACE solar wind monitor at the L1 point (220 Earth radii upstream from Earth), taking into account the time lag of about 1 hour, for the propagation time of the solar wind from ACE to Earth. Generally, the Lunar Prospector magnitudes are larger than those of T96, but the directional agreement is very good, except for a few vectors where very small fields are predicted by T96. The difference in magnitude may be due to the assumed merit function in the T96 model, and to the sparse data coverage at lunar distances.

3.2. Internal fields of the South Pole-Aitken Basin

After removing the model of the external field from field profiles, the residual vector field data over the SPA basin region was reviewed on a day-by-day basis, retaining only those days in which stacked profile plots of the internal field showed signficant pass-to-pass coherence. Fields of internal origin will usually appear on multiple passes because the separation of adjacent passes is most often less than or equal to the altitude above the surface. The profiles were separated into ascending (Figure 2a, and supplemental Figure S1) and descending (not shown, but similar and sparser) orbits as stacked profile plots. The arcuate features seen in the radial and theta components of the field are seen in all regimes (sun, shade, solar wind, magneto-tail, ascending, descending, at all altitudes, and in the scalar data, dependent only on spatial coverage). The resulting data have been used in a least- squares sense to characterize the internal, crustal field via a grid of dipoles [*Dyment and Arkani-Hamed*, 1998; *Purucker et al.*, 1996] extending over the entire region shown in the figure. A spherical coordinate system has been used throughout.

The internal field solution is then used to recalculate the magnetic field at a constant altitude of 30 km (Fig. 2b, and supplemental Figure S2). On this gnomonic projection, great circle arcs plot as straight lines. Notice that there is a dominant set of structures trending WNW covering much of the 1000 km wide region, and that there are secondary structures intersecting this dominant set. Arcuate features can also be clearly seen running E-W through the center of SPA. (Fig 3a). These arcuate features are absent from the easternmost and southernmost boundaries of SPA.

These features show no first-order correspondence to any surface topographic or structural feature on the lunar far side, suggesting that they represent features originating below the surface in the crust or mantle. The origin of these magnetic features within the crust, and not on the surface of the Moon, suggests that these features originated in a primordial lunar magnetic field, as cooling below the Curie temperature (the temperature above which materials lose their ability to sustain a remanent or induced magnetic field) locked in a magnetic remanence. The magnitude of the SPA magnetic feature was first recognized with the Apollo 15 subsatellite [*Coleman et al.*, 1972] but the subsatellite track was approximately parallel to the major linear features here, so that they could not be recognized. The reason for the absence of the cross-cutting features in the ER data remains unknown, although the footprint of the ER data can have significant errors in regions of high crustal field such as SPA.

4. Interpretation of the magnetic lineations

The proximity of these magnetic lineations to the South Pole-Aitken basin suggests that the lineations may be related to the formation of the basin or its subsequent history. Preservation of magnetic fabric dating from early crustal formation processes seems unlikely, due to the physical disruption of crustal target material by the impact and the likelihood that the event would tend to demagnetize and destroy magnetic lineation coherency in the immediate vicinity of the impact, as is thought to have occurred on Mars [*Acuña et al.*, 1999]. Subsequent to the formation of the South Pole-Aitken basin, the major events in the history are the formation of additional craters and small basins in the basin interior and rim (e.g., Poincare, Antoniadi, Apollo, Van de Graaff, Aitken and many

others) and the formation of the Orientale basin to the east and deposition of Orientale ejecta and crater chains in the interior of SPA [e.g., [*Stuart-Alexander*, 1978; *Wilhelms and Wilshire*, 1979; *Wilhelms*, 1987]. Emplacement of mare basalts on the SPA basin floor occurred well after basin formation and thus mare basalt eruptions tended to pond within the many craters that formed between the time of the impact and the volcanic flooding, and in other low-lying intercrater areas (Fig. 3b). Unlike the larger nearside maria, such as Imbrium and Serenitatis, which are characterized by widespread, continuous and thick mare deposits (e.g., [*Head and Wilson*, 1992; *Wilhelms*, 1987], SPA is incompletely flooded and has a patchy mare distribution, more similar to that in the Australe basin (e.g., [*Whitford-Stark and Head*, 1979]). *Yingst and Head* [1997] mapped 52 mare ponds in the South Pole-Aitken Basin, with a mean pond area of 2000 sq km, and a mean volume of 860 cubic km. They interpreted the ponds to be due largely to single eruptive phases that were emplaced through dikes directly from mantle sources without shallow crustal magma reservoirs and staging areas. *Yingst and Head III* [1999] examined the spectral characteristics of 21 of the mare ponds in SPA and found that their affinities were consistent with nearside basalts emplaced in the Late Imbrian Period (3.8-3.2 Ga). Information on the lunar magnetic field and its history was obtained from measurements of the paleointensity of returned samples; these measurements [summarized in [*Fuller and Cisowski*, 1987]] suggest that the Moon possessed a surface field of intensity comparable to that of present-day Earth for a period of time from about 3.6 to 3.8 billion years ago. Although the small size of the mare ponds and the lack of appropriate image data have precluded the derivation of direct crater size-frequency distribution dates for the ponds,

the general stratigraphic dating [*Wilhelms and Wilshire*, 1979; *Wilhelms*, 1987] and the spectral affinity with nearside Late Imbrian basalts [*Yingst and Head III*, 1999] both are consistent with the mare ponds having been emplaced during the time of the peak magnetic field (3.8-3.6 Ga). Examination of the location of the magnetic lineations shows some positive correlation between their concentration (Fig. 3a) and mare pond locations (Fig. 3b). Furthermore, the magnetic lineations cross specific mare ponds in some locations (compare Fig. 3a, b, and see supplemental Figure S3). For example, one prominent linear anomaly trends ESE and crosses mare patches in Van de Graff (v), Leeuwenhoek (L), and Apollo (P), and trend-parallel graben and mare-related dark-halo craters on the floor of Oppenheimer [*Head et al.*, 2000]. Another major linear trend (NNE) crosses the largest occurrence of mare in SPA (Mare Ingenii/Thomson (m)) and mare patches in Garavito (G), Hopmann (H), SW Van de Graaff, and Aitken. Other linear trends also show correlations with mare patch occurrences. Not all magnetic lineations are associated with mare ponds. In this scenario, not all intrusions reached the surface and resulted in mare ponds. In addition, not all mare ponds possess a magnetic signature. This suggests that the mare ponds represent a range of ages. Theoretical analyses of the ascent and eruption of magma, combined with observations of shallow dike intrusions and related deformation on the Moon [*Wilson and Head*, 1981; *Head and Wilson*, 1992] suggest that mare basalts were emplaced in blade like dikes with dimensions of several tens to many hundreds of kilometers length and tens to 200 m width. Dikes tend to approach the surface from depth with a broad convex-upward shape, and magma eruption usually takes place at the point where the convex portion of the dike first intersects the surface.

A magnetized dike was previously suggested as a source of the magnetic signature near the Rima Sirsalis rille [*Anderson et al.*, 1976]. More recent work has cast some doubt on this particular case [*Hood et al.*, 2001; *Halekas et al.*, 2001], but the new results presented here strengthen the general case for the existence of magnetized dikes on the Moon.

5. Conclusions

In summary, a number of lines of evidence support an interpretation of the linear magnetic anomalies as the manifestation of magnetized dikes related to the ascent of magma and emplacement of mare basalts on the floor of the South Pole-Aitken basin: 1) the linear nature of the magnetic anomalies and the linear nature of dikes, 2) the concentration of the anomalies in the center and NW portions of the basin where the mare ponds are also concentrated, 3) the coincidence of some magnetic lineation locations with specific basaltic ponds, 4) the candidate width and depth range of the mare pond feeder dikes and the strength of the magnetic lineations, and 5) the consistency of the age of the emplacement of the feeder dikes/basaltic ponds and the time of peak lunar magnetism. Thus, we interpret the linear magnetic anomalies to have formed by dikes that emplaced many of the mare ponds on the floor of SPA, with solidification of the dikes taking place during the time of the peak magnetic field, about 3.6-3.8 billion years ago. The distinctive nature of the anomalies may have been enhanced by a strong magnetic contrast between the dikes and lower crustal material, either non-magnetized, or demagnetized by the earlier SPA basin-forming event.

6. Acknowledgments

We would like to thank the NASA Planetary Data System node at the University of California, Los Angeles for the provision of the Level 1B magnetic field data. We thank the National Aeronautics and Space Administration, Space Sciences Directorate, Solar System Exploration Division for financial support (Planetary Geology and Geophysics Program grant NNG05G121G to JWH).

References

Acuña, M. H., et al. (1999), Global distribution of crustal magnetization discovered by the Mars Global Surveyor MAG/ER experiment, *Science*, *284*, 790–793.

Anderson, K. A., R. P. Lin, R. E. McGuire, J. E. McCoy, C. T. Russell, and J. P. J. Coleman (1976), Linear magnetization feature associated with Rima Sirsalis, *Earth. Planet. Sci. Lett.*, *34*, 141–151.

Blakely, R. J. (1995), *Potenial Theory in Gravity and Magnetic Applications*, 441 pp pp., Cambridge.

Coleman, P., C. Russell, L. Sharp, and G. Schubert (1972), Preliminary mapping of the Lunar magnetic field, *Phys.Earth Plan. Int.*, *6*, 167.

Dyment, J., and J. Arkani-Hamed (1998), Equivalent source dipoles revisited, *Geophys. Res. Lett.*, *25*, 2003–2006.

Fuller, M., and S. Cisowski (1987), Lunar paleomagnetism, in *Geomagnetism*, edited by J. Jacobs, chap. 2, pp. 307–456, Academic Press.

Halekas, J. S., D. L. Mitchell, R. P. Lin, S. Frey, M. H. Acuña, and A. B. Binder (2001), Mapping of lunar crustal magnetic fields using lunar prospector electron reflectometer

data, *J. Geophys. Res.*, *106*, 27,841–27,852.

Head, J., L. Wilson, and C. Pieters (2000), Pyroclastic eruptions associated with the floor-fractured lunar farside crater oppenheimer in the south pole-aitken basin, in *Lunar and Planetary Science XXXI*.

Head, J. W., and L. Wilson (1992), Lunar mare volcanism-stratigraphy, eruption conditions, and the evolution of secondary crusts, *Geochim. et Cosmochim. Acta*, *56*, 2155–2175.

Hood, L. L., A. Zakharian, J. Halekas, D. L. Mitchell, R. P. Lin, M. H. Acuña, and A. B. Binder (2001), Initial mapping and interpretation of lunar crustal magnetic anomalies using Lunar Prospector magnetometer data, *J. Geophys. Res.*, *106*, 27,825–27,839.

Maus, S., M. Rother, K. Hemant, C. Stolle, H. Lühr, A. Kuvshinov, and N. Olsen (2006), Earth's lithospheric magnetic field determined to spherical harmonic degree 90 from CHAMP satellite measurements, *Geophys. J. Int.*, *164*, 319–330.

Purucker, M., T. Sabaka, and R. Langel (1996), Conjugate gradient analysis: a new tool for studying satellite magnetic data sets, *Geophys. Res. Lett.*, *23*, 507–510.

Stuart-Alexander, D. E. (1978), *Geologic map of the central far side of the Moon*, I-1047, U.S. Geological Survey.

Tsyganenko, N. A. (1996), Effects of the solar wind conditions on the global magnetospheric configuration as deduced from data-based field models, in *European Space Agency Publ. ESA SP-389*, pp. 181–185.

Whitford-Stark, J. L., and J. Head (1979), Charting the southern seas: The evolution of the lunar mare australe, in *Lunar and Planetary Science VIII*.

Wilhelms, D. E. (1987), *The geologic history of the Moon*, Professional Paper 1348, 256-258 pp., U.S. Geological Survey.

Wilhelms, K., D. E. Howard, and H. Wilshire (1979), *Geologic map of the south side of the Moon*, I-1162, U.S. Geological Survey.

Wilson, L., and J. W. Head (1981), Ascent and eruption of basaltic magma on the Earth and Moon, *J. Geophys. Res.*, *86*, 2971–3001.

Yingst, R., and J. W. Head (1997), Volumes of lunar lava ponds in south pole-aitken and orientale basins: Implications for eruption conditions, transport mechanisms, and magma source regions, *J. Geophys. Res.*, *102*, 10,909–10,931.

Yingst, R., and J. W. Head III (1999), Geology of mare deposits in South Pole-Aitken basin as seen by Clementine UVVIS data, *J. Geophys. Res.*, *104*, 18,957.

Figure 1. T96 predictions (blue) and Lunar Prospector estimates (red) in Earth's magnetotail. The small green arrows represent the induced component associated with the estimates of the external field. The subsatellite location of these traverses covers the South Pole-Aitken (SPA) basin between 180 and 192 degrees Longitude. Geocentric Solar Ecliptic (GSE) coordinates.

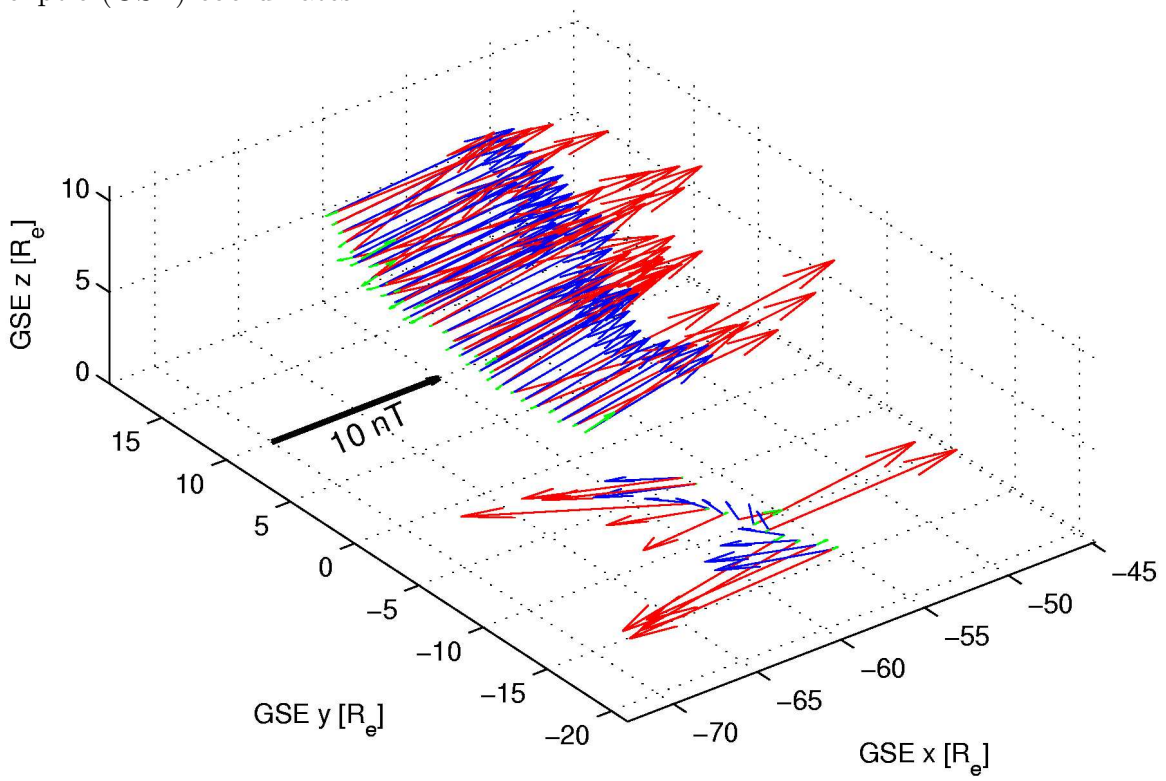

Figure 2. (A)Stacked profile plot of the radial (B_r) magnetic field associated with ascending passes over the northern boundary of the SPA basin region. The profiles are shown after external field model removal. Median altitude = 31 km. Red is positive, blue is negative. 15 nT scale bar shown at bottom of plots. The -2 km elevation contour is shown as a solid black line, outlining the SPA basin. (B) Altitude normalized B_r magnetic fields calculated at 30 km altitude, shown on a gnomonic projection. The symbol m locates the largest outcrop of mare ponds (Mare Ingenii/Thomson) in the SPA basin.

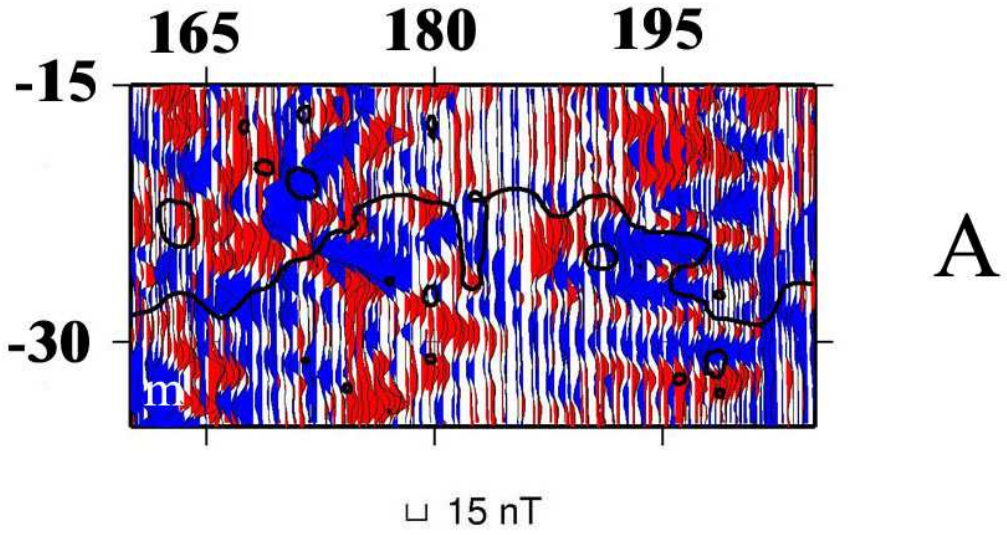

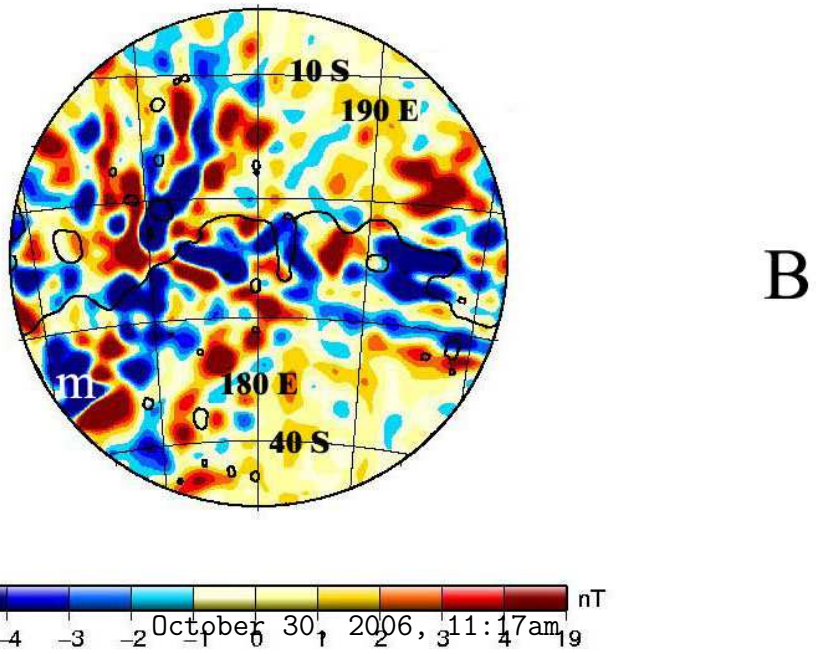

Figure 3. (A) Altitude normalized B_r magnetic fields calculated from ascending data at 30 km altitude over the entire SPA region, shown on a cylindrical equidistant projection. The -2 km elevation contour is shown as a solid black line, outlining the SPA basin. (B). Airbrush shaded relief USGS map of the SPA region, with mare ponds shown in black. Outline of SPA sketched as a solid dark line. Same projection and area as A. The following mare ponds are labeled: Mare Ingenii/Thomson (m), Garavito (G), Hopmann (H), Van de Graff (v), Leeuwenhoek (L), and Apollo (P).

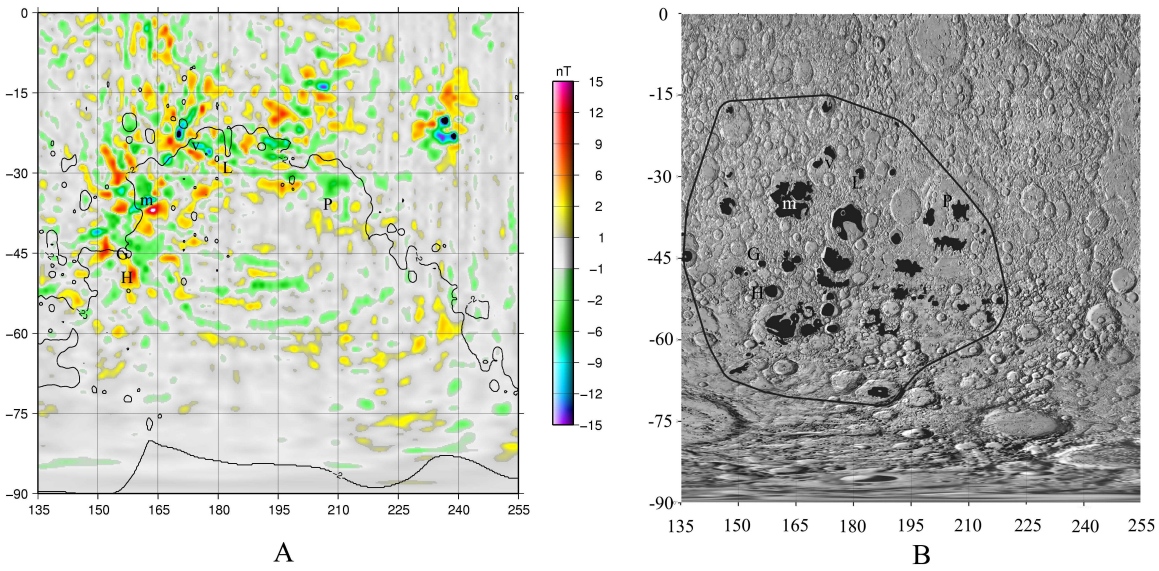

Figure S1. (A)Stacked profile plots of ascending passes showing the actual magnetic field data after external field model removal (left), the modeled internal component (center), and the remaining unfit field (right) above the northern boundary of the SPA basin region. The three components shown are B_r (top), B_θ (center), and B_ϕ (bottom). Red is positive, blue is negative. 15 nT scale bar shown in bottom right hand corner.

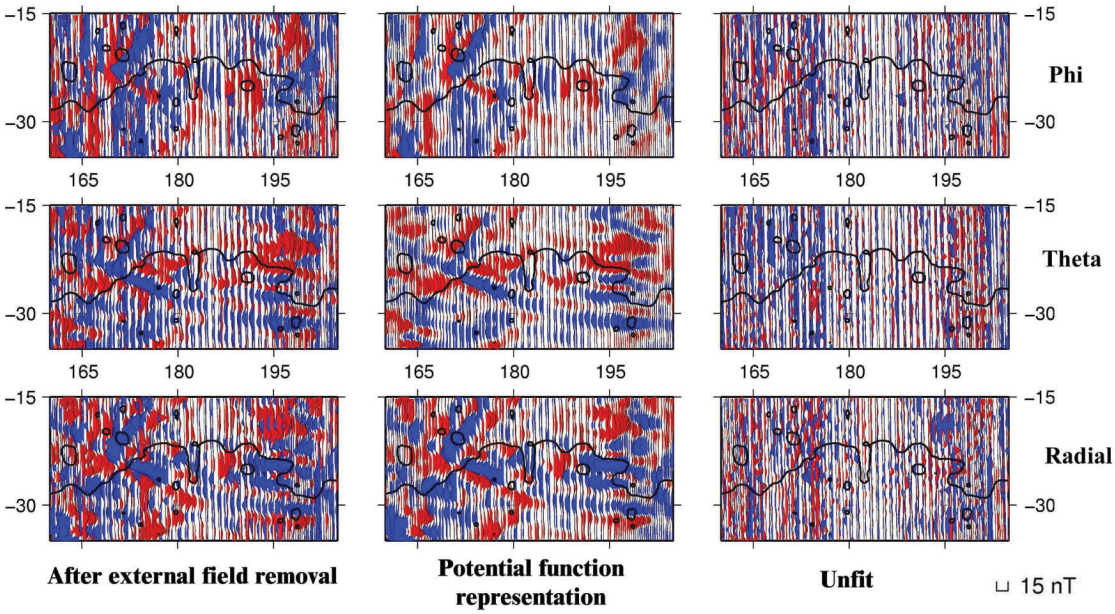

Figure S2. Altitude-normalized B_r (bottom), B_θ (center), and scalar magnitude fields (top) calculated after removal of a uniform external field (left) using the techniques discussed in this paper and after quadratic detrending (right), using data selected and detrended by L. Hood (personal communication). Altitude normalization technique applied to both data sets is identical. Fields shown on a gnomonic projection at 30 km altitude.

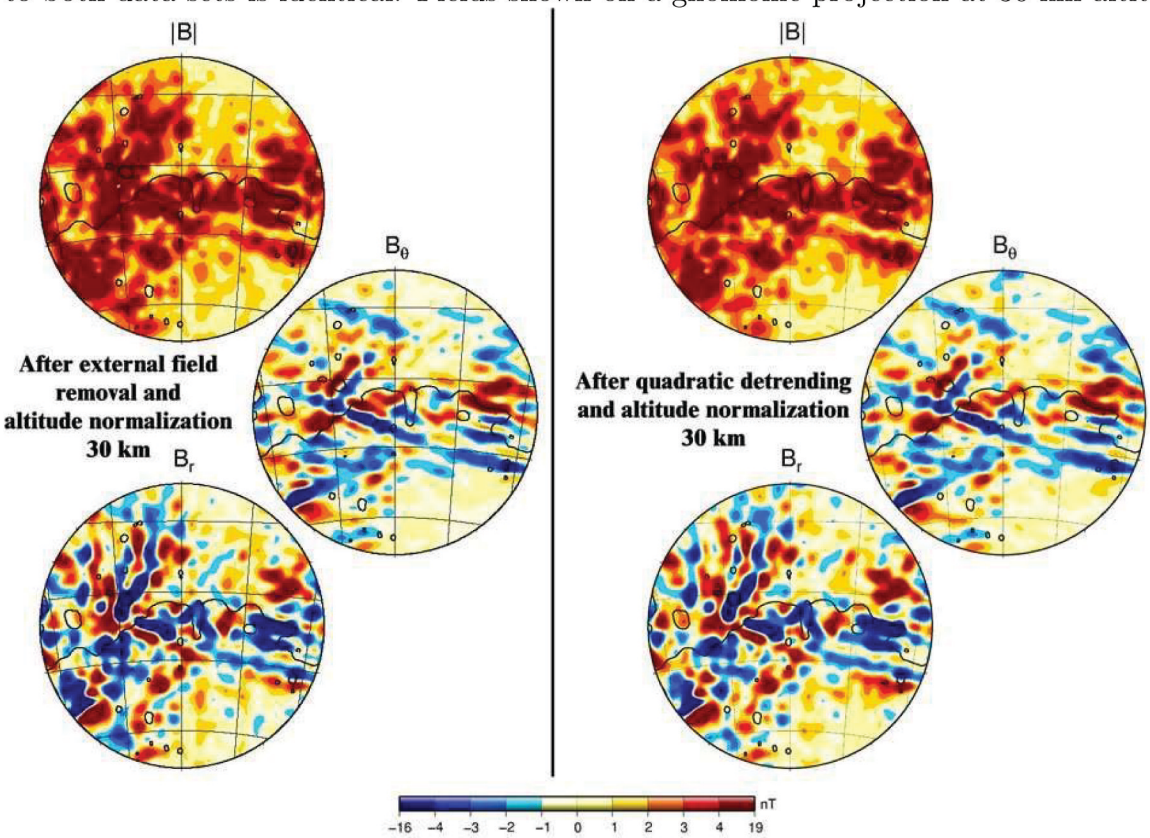

Figure S3. Figures 3a and 3b, merged.